Available online at www.sciencedirect.com
SCIENCE DIRECT®
Carbon 44 (2006) 231–242
CARBON
www.elsevier.com/locate/carbon

Density functional study of graphite bulk and surface properties

Newton Ooi *, Asit Rairkar, James B. Adams

Department of Chemical and Materials Engineering, P.O. Box 876006, Ira A. Fulton School of Engineering and Applied Sciences, Arizona State University, Tempe, AZ 85287-6006, USA

Received 15 May 2005; accepted 24 July 2005
Available online 13 September 2005

Abstract

The structural and electronic properties of bulk graphite were compared using density functional theory calculations with the local density (LDA) and generalized gradient (GGA) approximations to determine the relative ability of each to model this material. The GGA fails to generate interplanar bonding, but the LDA does, even though the band structures obtained from both approximations were essentially identical. The atomic geometry, electronic structure, and enthalpy of the graphite (0 0 0 1) surface were then obtained using the LDA. The calculated surface energy was ~0.075 J/m^2 and the calculated work function was in 4.4–5.2 eV range, both of which correspond well to published, measured and calculated values. The surface is semi-metallic, just like in the bulk, with the conduction band minimum and valence band maximum just touching with minimal overlap in the H–K region in the Brillouin Zone, so the electron affinity was identical to the work function. The (0 0 0 1) surface undergoes no noticeable relaxation and no reconstruction, as the strong covalent bonding prevents any corrugation of the basal planes.

Keywords: Graphite; Computational chemistry; Electrical (electronic) properties; Electronic structure; Surface properties

1. Introduction

Graphite is widely used as a solid lubricant [1,2] for preventing wear and abrasion and can also be dispersed in water and organic fluids to make a liquid lubricant. Graphite is soft, smooth, inflammable, nontoxic, is inert in ambient air, does not emit fumes, and has a low coefficient of friction. It is cheaper and environmentally safer to produce and use than many other tribological coatings and lubricants such as polymers, diamond, DLC, and the various borides, nitrides and carbides. It does not react with most metals and metal oxides below the other material's melting point. It resists corrosion by most liquids below 600 K and has a melting point of 3800 K, higher than many metals and alloys. This high melting point and chemical inertness make it commonly used as crucibles for holding molten metals. Graphite coatings can be deposited using laser ablation, chemical vapor deposition, thermal spraying, or as a painted film [3]. Composites of graphite and other materials such as brass, diamond, Si, and SiC have improved mechanical properties making them optimal coating materials [4].

Graphite [5] occurs in two crystal phases: hexagonal (α) and rhombohedral (β). The former is more abundant in nature, is known as the Bernal phase, and is the subject of this report. In-plane bonding is purely covalent and inter-planar bonding is weak van der Waals. Graphite comes in several forms. Polycrystalline graphite has a discernible grain structure with some open porosity. Single crystal graphite is often called highly orientated pyrolytic graphite (HOPG), has highly anisotropic properties, and is formed by hydrocarbon cracking. Vitreous or amorphous graphite has a density <2.0 mg/m^3, and its structure resembles a tangle of graphitic ribbons that are only a few unit cells thick.

* Corresponding author. Tel./fax: +1 480 965 8509.
E-mail address: newton.ooi@asu.edu (N. Ooi).

0008-6223/$ - see front matter © 2005 Elsevier Ltd. All rights reserved.
doi:10.1016/j.carbon.2005.07.036

There have been many published simulations on the properties of graphite using the Hohenberg–Kohn–Sham formulism of density functional theory (DFT), yet there are still several questions that are not fully resolved. First, all relevant publications state that the LDA (local density approximation) exchange–correlation functional is better than any GGA (generalized gradient approximation) for simulating graphite, yet there is little literature showing how or why. Second, there has been much research into how well different pseudopotentials (PP) model specific groups of elements (i.e. oxygen, f-shell metals) in the Periodic Table, and developing PP specifically to handle these elements. Yet, we could not find any work that compared the properties of graphite obtained with different PP. Third, there is remarkably little ab initio literature on its surface properties given its prevalent use. Last, we could not find any experimental or theoretical data on whether the graphite surface relaxes or reconstructs.

We have therefore used first-principles atomistic scale simulations to study the properties of both bulk and surface graphite to address the issues listed above. Specifically, calculations will be done using both the LDA and GGA, using two different types of PP.

2. Literature review of graphite simulations

Common versions of both the LDA and GGA are time-independent; hence they cannot reproduce dynamical, time-dependent processes, such as van der Waals bonding. Therefore, ab initio modeling of graphite has been the focus of much discussion and innovation. Girifalco et al. [6] examined the literature to determine the important factors others found in modeling the binding between graphene (basal) planes. They concluded that LDA–DFT can produce inter-layer binding in graphite that gives lattice constants and other properties similar to experiment, even though it is not van der Waals bonding per se. He breaks down the interplanar bonding into an attractive and a repulsive part. The former has two components: a decrease in kinetic energy due to delocalization of the p_Z electrons between adjacent planes, and an interaction between fluctuating dipoles on C atoms in adjacent planes (van der Waals component). The repulsive part arises from overlap of electrons on adjacent graphene planes.

There have been attempts to generate an XC functional that does reproduce van der Waals bonding. Rydberg et al. [7] developed a fully non-local XC functional as compared to the LDA (local) and GGA (semi-local), though their calculated lattice constants for graphite using this functional are 0.5 Å worse than the best LDA calculations. A commonly shared conclusion in the literature is that the LDA does better than the GGA in modeling of graphite, though there is minimal demonstration in the literature [8]. Recent DFT calculations of bulk graphite properties match experimental values well and a brief summary of some of them (all LDA) is provided here.

Charlier et al. [9] examined the band structures for graphite with three different stacking sequences: AA, AB (Bernal) and ABC (rhombohedral). The differences were used to resolve discrepancies in experimentally measured graphite band structures. Specifically, natural graphite is a mixture of all the three allotropes, so its band structure will not correspond exactly to that of the Bernal structure. There are several publications comparing the properties of graphite with diamond, and examining the phase transition between them. Two recent studies by Furthmuller et al. [10] and Janotti et al. [11] showed that graphite is more stable than diamond at low temperature and pressure, as known experimentally.

Graphite is a thermal and electrical conductor along the basal planes but an insulator perpendicular to the basal planes, and is alternatively considered a semi-metal or a zero-gap semiconductor. Heske et al. [12] addressed this issue by comparing calculated results with photoelectron spectroscopy experiments. Discrepancies between the two were explained in terms of many-body effects. Schabel et al. [13] also studied the graphite band structure, and compared their data with experiments and other theoretical predictions. Differences between the band structures from different publications were highlighted and attributed to factors such as the k-mesh used, the pseudopotential used and other simulation parameters.

Wang et al. [14] examined inter- and intra-layer bonding in graphite and graphitic silicon using pseudopotential calculations. Plots of the charge density arising from different bands showed that the p_Z electrons contribute to in-plane bonding along with providing interplanar van der Waals bonding. The in-plane bonding strength is reduced in Si, and interplanar bonding is enhanced due to formation of covalent bonds between atoms on adjacent planes. Boettger [15] determined the band structure, lattice constants, and elastic constants of graphite using all-electron calculations. Of the five independent elastic constants calculated, four were close to experimental values, while C_{13} was negative and $\sim$0, in contrast to the slightly positive experimental value. This discrepancy was attributed to the inability of LDA to reproduce van der Waals bonding.

The graphite ring occurs commonly in organic chemistry as part of many organic molecules such as benzene, and has been studied extensively using techniques more common in chemistry. Chen and Yang [16] performed Hartree Fock (HF) and DFT calculations using graphite models that were single-layer sheets ranging in size from 1–7 adjacent rings within one plane. The ring edges were terminated with hydrogen atoms. Bond lengths, angles, and order, and Raman frequencies were calculated for

the different size models to determine how different sized models reproduced results for bulk graphite. Butkus et al. used HF theory and cluster models to study bulk graphite, the graphite (0001) surface [17] and several prismatic surfaces [18]. Their work did not calculate many material properties, and instead focused more on the wave functions used in the calculation, and how this affected bonding characteristics between atoms.

3. Methodology

We performed our calculations using the Vienna Ab initio Software Package (VASP) [19]. The single-particle Kohn–Sham functions were expanded in a plane-wave basis set. Pseudopotentials [20,21] were used to represent the core electrons and nucleus of an atom. VASP provides ultra-soft (US) pseudopotentials developed by Vanderbilt [22] and all-electron projected augmented wave (PAW) potentials [23,24]. Energies of the irreducible Brillouin zone (IBZ) were sampled with a Γ-centered grid of k-points. Exchange and correlation was approximated using either the LDA adapted by Ceperly and Alder [25], or the GGA of Perdew and Wang [26]. Ground state energies and charge densities were calculated self-consistently using a Pulay-like mixing scheme [27–29] and either the conjugate gradient algorithm or the residuum minimization method by direct inversion in the iterative subspace [30,31]. Initial charge densities were taken as a superposition of atomic charge densities. Atomic positions were relaxed to their ground state by minimizing their Hellman–Feynman forces [32,33] using the conjugate gradient algorithm such that all interatomic forces were less than 0.1 eV/Å.

4. Bulk calculations

The Bernal structure unit cell contains four carbon atoms with experimental lattice constants of $a_0 = 2.46$ Å, $c_0 = 6.78$ Å [34]. Calculations were performed on this unit cell to determine which potential gave bulk properties closer to experiment. This potential would then be used for the surface calculations. There is minimal proof in the literature as to why the LDA is better than the GGA in modeling of graphite, so we performed bulk calculations using the GGA and the LDA to determine which is better. Convergence of k-point sampling to 1 meV/atom was reached with an $8 \times 8 \times 8$ grid and 50 points in the IBZ for both the GGA and LDA. In graphite each atom is sp^2 hybridized, and all the valence electrons have the same spin, so calculations on the unit cell gave identical energies with or without spin polarization, and the unit cell has a magnetic moment = 0. Further calculations did not use spin polarization to reduce computational cost (see Fig. 1).

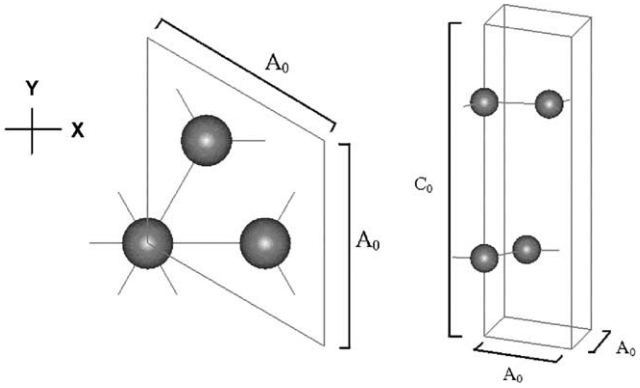

Fig. 1. Graphite unit cell.

Plane wave convergence to 2 meV/atom was reached at 400 eV using the GGA PAW. The enthalpy (H) is calculated at a series of cell volumes and the resulting curve is fitted with the Birch–Murnaghan [35] equation of state to determine the bulk modulus (B_0), lattice constants, and cohesive energy (E_C). The enthalpy versus volume (H–V) test for non-cubic systems such as graphite is different from cubic systems. Two options are possible. First, each lattice constant can be varied separately. This is more thorough but can lead to a final structure that does not exist experimentally. Second, a_0 and c_0 can be varied together. The second method was used because it requires fewer calculations and at each volume increment, the cell shape and atom positions were relaxed. The volume of a hexagonal cell = $V = 0.5(3^{1/2})a_0^2 c_0$.

Fermi level smearing is recommended for calculations on metals, but not for non-metals. Since graphite is a semi-metal, calculations were performed both with and without smearing for comparison. Two parallel tests of H–V were performed using the GGA PAW. The first test used the linear tetrahedron method with Bloch corrections [36] (no smearing), and the second used 0.1 eV Methfessel–Paxton [37] smearing. In each test, the cell at each volume increment was minimized in three sequential calculations, where atom positions and cell shape were free to vary in each one. Therefore, at each volume, the unit cell was minimized and the output structure was used as the input structure of a second minimization. The output structure from this second minimization was used as the input structure into a third and final minimization. The H and cell parameters from this final minimization were used to generate the H–V curve. The same volume increments were used for calculations both with and without smearing. The H never reaches a minimum for either test (Fig. 2a), thereby demonstrating that the GGA fails to reproduce bonding in graphite, specifically interlayer bonding.

The H–V test was repeated using the LDA US and LDA PAW. Plane wave convergence to 2 meV per atom was reached with a 300 eV (400 eV) cutoff for the LDA

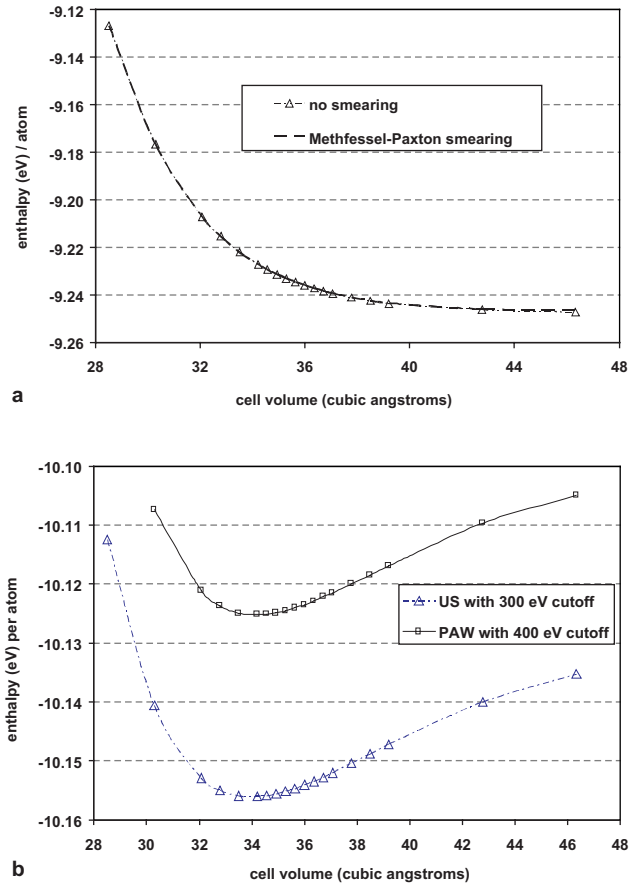

Fig. 2. Enthalpy versus volume test for graphite: (a) GGA PAW enthalpy versus volume and (b) LDA enthalpy versus volume.

US (LDA PAW). At each volume increment, the cell shape and atom positions were allowed to relax in three sequential calculations in the same manner as the GGA PAW. Each calculation was run twice; once without smearing, and once using 0.1 eV Methfessel–Paxton smearing. As seen in Fig. 2b, both US and PAW potentials give a minimum H for $V \sim 34.2$ Å^3 with $a_0 = 2.44$ Å, and $c_0 = 6.63$ Å, demonstrating that the LDA does reproduce bonding of the right magnitude in graphite, though it might not be van der Waals bonding. The cohesive energy, E_C, which is the energy needed to remove an atom from the bulk and place it infinitely far away, was calculated using Eq. (1) where H_C is the spin-polarized enthalpy of the free carbon atom.

$$E_C = (H/4) - H_C \quad (1)$$

The cell shapes obtained by the Birch–Murnaghan fits for both LDA potentials were relaxed one final time allowing atom positions and cell shape to vary. Results are provided in Table 1. The a_0, c_0, and B_0 are similar to experimental values, but the calculated cohesive energies are larger than the experimental value by ~20%. This discrepancy is typical of LDA calculations. Experimental values were measured ~300 K, whereas our simulations are at 0 K. Graphite has a coefficient of thermal expansion (averaged over both axes) of 7.1×10^{-6}/K at room temperature [1], so the graphite cell will be slightly smaller at 0 K than at 300 K, which is matched by our calculations. The LDA US and PAW give similar values of lattice constants, E_C and B_0 so either can be used for surface calculations.

Table 1
Graphite bulk properties

Source	a_0 (Å)	c_0 (Å)	V_0 (Å^3)	E_C (eV)	B_0 (GPa)
LDA PAW	2.448	6.582	34.16	8.89	30.30
LDA US	2.443	6.575	33.98	8.79	28.98
Experiment ~300 K [38]	2.46	6.71	35.28	X	X
Experiment ~300 K [39]	2.603	6.706	35.12	X	33.8
Experiment ~300 K [40]	2.462	6.711	35.638	X	X
Experiment ~300 K [41]	X	X	X	7.37	X
Calculation at 0 K [Boettger]	2.448	6.784	35.208	8.87	38.3
Calculation at 0 K [42]	2.443	6.679	34.508	9.00	288

4.1. Bulk electronic structure

Documented PP calculations of graphite in the literature have used norm-conserving or US PP with the LDA [9,13,14,42,43]. This current work is the first to compare properties using different PP, specifically PAW versus US, for both the LDA and GGA. The electronic structure of graphite was examined by looking at its density of states (DOS) and band diagrams calculated by both LDA and GGA, for both PAW and US PP. The DOS was examined for the unit cell and as projected onto each of the four atoms in the unit cell. The H–V curve for the GGA PAW did not predict an equilibrium structure, and the LDA US and PAW predict different ground state lattice constants, so the issue arises as to what structure(s) to calculate the electronic structure for. This was resolved by obtaining the DOS and band diagram on a unit cell using the experimental lattice constants of $a_0 = 2.46$ Å and $c_0 = 6.78$ Å for all four XC-PP combinations: LDA PAW, LDA US, GGA PAW, and GGA US. For comparison, the electronic structure was also obtained for the LDA PAW and US using our calculated lattice constants. The electronic structure obtained at the calculated a_0 and c_0 were very similar to that obtained at the experimental lattice constants so all further discussion and figures are for the data obtained using the experimental a_0 and c_0.

To obtain high accuracy, the DOS was obtained in a calculation using a $15 \times 15 \times 15$ k-mesh of 216 irreducible points. The charge density and wave functions from this calculation were used as input in a subsequent calculation to obtain the band structure at all high symmetry points and along all high symmetry directions. This latter calculation at specific points precludes the use of space-filling tetrahedrons in the BZ, so the tetrahedron

method cannot be used, and 0.01 eV smearing was used instead. All eigenvalues and occupations of the occupied and first 12 unoccupied bands were identical for both Gaussian and Methfessel–Paxton smearing, hence their band diagrams are also identical.

There are two atomic environments in graphite due to its ABAB stacking. One environment, which we refer to as type 1, is where the atom is directly above and below atoms in the adjacent planes. The other environment, type 2, is where the atom is not above or below atoms in the adjacent planes. Atoms in the two environments will be referred to as atom 1 and atom 2. The DOS of atoms 1 and 2 should be different because the p_Z orbital on atom 1 is interacting with the p_Z orbital on atoms in adjacent planes, whereas atom 2 is not interacting with atoms on adjacent planes. Fig. 3 provides the DOS calculated by the LDA PAW. The DOS for the unit cell shows two groups of peaks with a band gap of ~1 eV between them, and a vacuum level inside the conduction band (CB) near the CB minimum. The Fermi energy (E_F) is placed at the top of the valence band (VB) so all states below it have two electrons per orbital, and all states above it are unoccupied.

The projected DOS (PDOS) on either atom when divided into contributions from each angular momentum shows several peaks. The 1 s core state is lowest in energy and resides in the −8 to −15 eV range. The second group of peaks is the $2sp^2$ hybridized states and the $2p_Z$ orbital, with the latter being higher in energy such that it provides the upper bound of the VB. The CB states are composed of two parts: a $3p_Z$ orbital, and a $3sp^2$ state formed by $3s + 3p_X + 3p_Y$ hybridization. Therefore, the $n = 3$ orbitals hybridize in a similar fashion as the $n = 2$ orbitals. The DOS of atom 1 is different from the DOS of atom 2 because on atom 1, the $2p_Z$ and $3p_Z$ states are about equal in height, whereas on atom 2, the $3p_Z$ is higher than the $2p_Z$ state. This seems to indicate that interplanar bonding in graphite is partially due to interactions between $3p_Z$ orbitals of atoms on adjacent planes.

The bulk DOS calculated by the GGA PAW is similar to that obtained by the LDA PAW; see Fig. 4. Peak shapes and positions are nearly identical between the two, with both showing a zero band gap without any overlap between the CB and VB. The difference is in the vacuum level, with it being above the entire CB in the GGA DOS, but inside the CB in the LDA DOS. The PDOS calculated by the GGA PAW has peak shapes and positions similar to the PDOS calculated by the LDA PAW for both atoms 1 and 2. Again the difference between the DOS for atoms 1 and 2 is that the $3p_Z$ peak is higher on atom 1 than on atom 2, similar to that found for the LDA PAW. Because the *lm*-decomposed DOS is so similar to the LDA PAW data, the PDOS using the GGA PAW is shown differently; specifically, it is decomposed into the *l*-components only, so the total DOS in the s and p orbitals are shown.

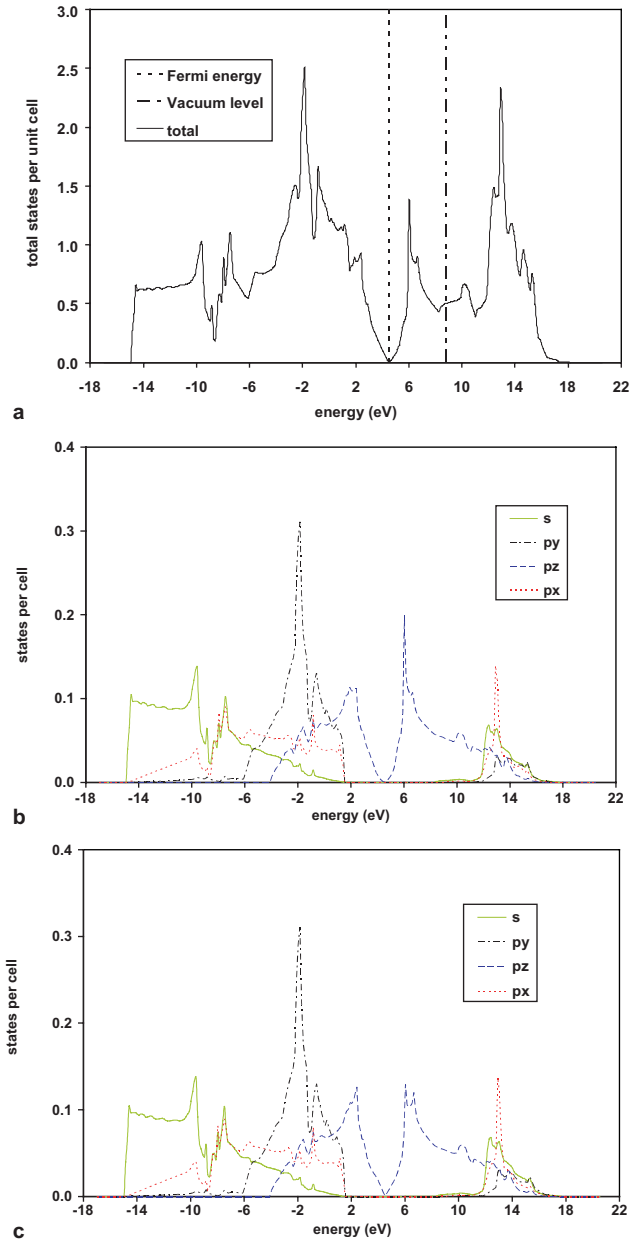

Fig. 3. Graphite DOS calculated using LDA PAW: (a) DOS for the unit cell, (b) projected DOS on atom 1 and (c) projected DOS on atom 2.

The DOS as calculated for the US using the LDA/GGA share several similarities with that obtained using the PAW and so are not shown. First, peak shapes, widths, and positions are very similar for both the cell DOS and the PDOS on each atom. Second, the band gap is zero for all cases with no overlap, with the $2p_Z$ and $3p_Z$ orbitals contacting at the E_F. Third, all PDOS show the same $2s + 2p_X + 2p_Y$ hybridization in the VB, and the same $3s + 3p_X + 3p_Y$ hybridization in the CB, with the p_Z orbital higher in energy than the sp^2 orbitals in the VB, but lower in energy than the sp^2 orbitals in the CB. Fourth, the $3p_Z$ peak has a reduced intensity

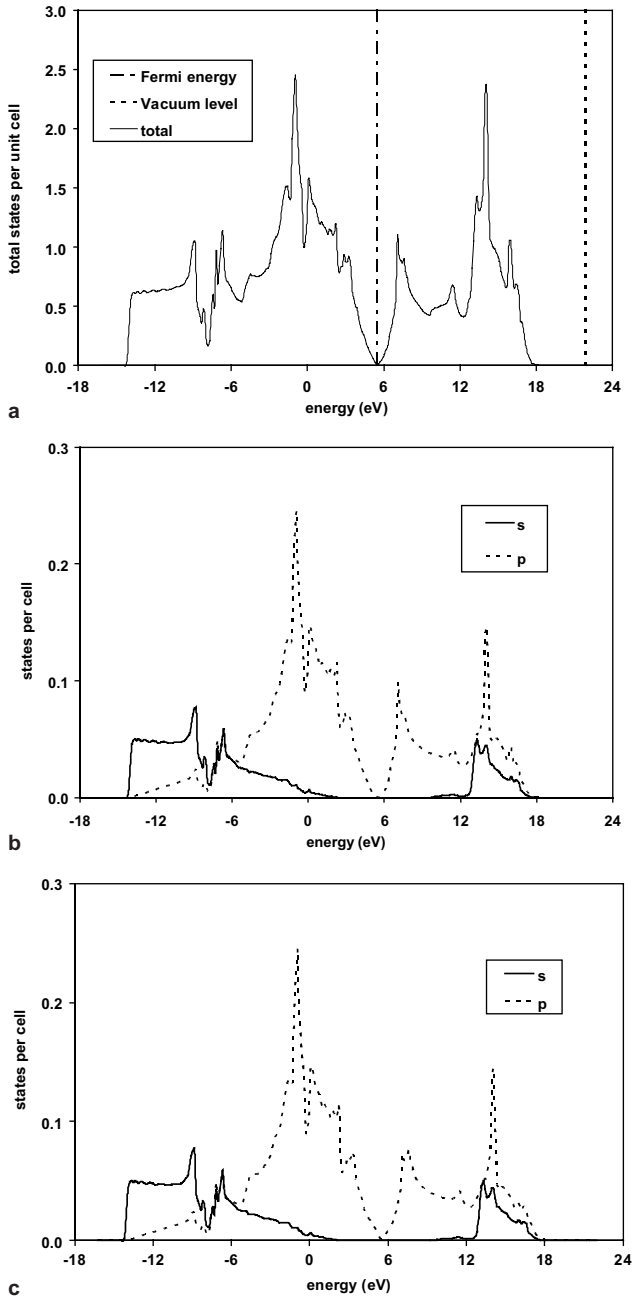

Fig. 4. Graphite DOS calculated using GGA PAW: (a) DOS for the unit cell, (b) projected DOS on atom 1 and (c) projected DOS on atom 2.

on atom 2 than on atom 1, whereas all the other peaks remain the same. The $2p_Z$ and $3p_Z$ orbitals represent the VB maximum and CB minimum, suggesting that electrical conduction in graphite occurs by electrons in the $2p_Z$ orbital jumping into the $3p_Z$ orbital and moving across the basal planes, consistent with the high electrical conductivity found along the basal planes experimentally.

There were two main differences between the DOS calculated by different XC functionals and PP. First, the vacuum level is above the entire CB for the GGA PAW, but is inside the CB closer to the band minimum for the other three XC–PP combinations. The reasons for this are still unclear. Second, all peaks obtained by the LDA PAW (US) are about 50% higher than the corresponding peaks in the GGA PAW (US) calculation, signifying weaker inter-atomic bonding in graphite as predicted by GGA versus LDA. This difference in peak magnitudes could be why the GGA fails to generate an interplanar attraction. A summary of the bulk electronic structure is given in Table 2.

The band diagrams generated by all four XC–PP combinations were very similar to each other and for the LDA, the band diagram obtained at the experimental a_0 and c_0 are nearly identical to that obtained at our bulk-predicted lattice constants; so only the data for the PAW calculations are shown. The dark bands are the VB and the light bands are the CB. They all show the VB and CB contacting along the $H \rightarrow K$ direction of the Brillouin Zone, which matches the common conclusion [9,15,44] in the recent literature. The E_F is shown as a light gray horizontal line (see Fig. 5).

5. Graphite (0001) surface

Graphite has two types of surfaces; the (0001) basal plane and the prismatic planes. The former is the lowest energy surface of graphite, and is more commonly observed, while the latter are normal to the basal plane. The (0001) surface energy (σ) is alternatively called the interlayer cohesive energy, interlayer binding energy, exfoliation energy, or basal cleavage energy in the literature. The primitive 1×1 model of the (0001) surface as shown in Fig. 1 has an AB stacking sequence with two atoms per layer. The area of one 1×1 surface is $A = (a_0)^2(3/4)^{1/2}$. Atomic relaxations used 0.1 eV Methfessel–Paxton smearing, and single point energy (SPE) calculations used no smearing.

5.1. Surface convergence tests

Initial surface calculations were performed on a 1×1 2-layer slab (4 atoms total) constructed with lattice constants obtained from the bulk LDA H–V tests. k-Point convergence was reached with an $11 \times 11 \times 2$ grid and 32 irreducible points. Vacuum thickness convergence

Table 2
Band properties (eV) using different XC functionals and pseudopotentials

Potential	Cutoff energy	VB min	CB max	E_F	Vacuum
LDA PAW	400	−14.84	18.53	4.51	8.7931
LDA US	300	−15.67	18.00	3.78	8.0726
GGA PAW	400	−14.17	20.06	5.48	21.875
GGA US	300	−15.59	19.96	3.95	8.2165

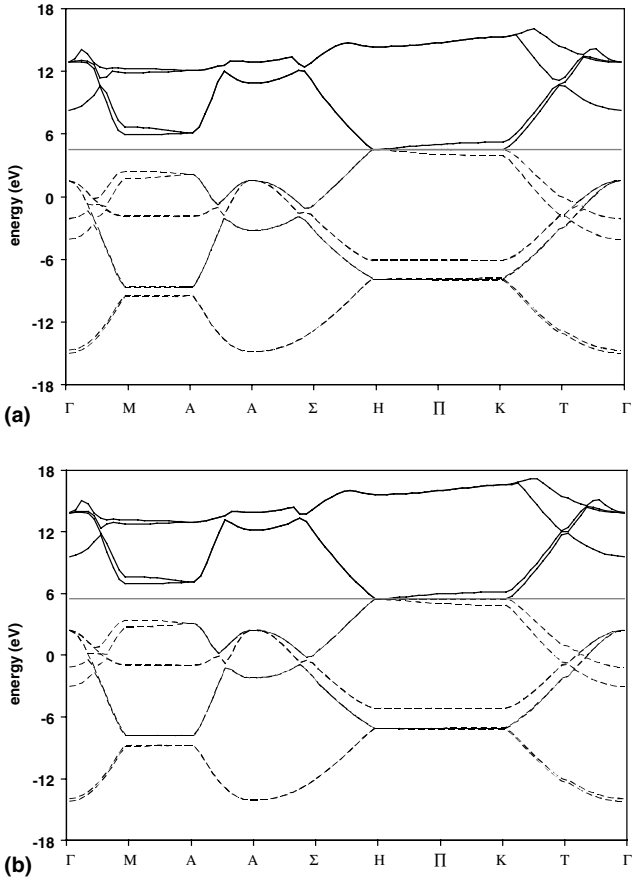

Fig. 5. Band diagram calculated using experimental lattice constants: (a) LDA PAW and (b) GGA PAW.

was reached at 10 Å. Starting with a 1-layer slab, the slab thickness was converged by adding one atomic plane at a time and calculating σ at each thickness up to a maximum thickness of 14 atomic planes. At each slab thickness, the SPE was obtained first for the as-built slab, all atom positions were then relaxed such that all forces were less than 0.05 eV/Å and an SPE was calculated on the relaxed slab. This was repeated for both the PAW and US. No relaxations or reconstructions occurred for any of the slabs, regardless of slab thickness, for both US and PAW, so within the precision of the calculations the relaxed slabs were identical to the as-built slabs in both atomic geometry (precise to 10^{-6} Å), total energy (precise to 10^{-6} eV), and hence, σ (precise to 10^{-6} J/m^2). This makes sense as the graphite intra-planar bonding is extremely strong, preventing any buckling from occurring.

The σ was calculated using two different equations for comparison; see Table 3. The first is the classical equation, where σ is the energy of a slab + vacuum (E_{surface}) minus the energy of a bulk slab having the identical number of atoms (E_{bulk}). The factor of 2 adjusts for the slab having two faces, the top and the bottom, each with an area = A. This equation always works for classical simulations, but does not always work for calculations where electrons can flow and form a dipole moment (quantum calculations).

Table 3
Calculated graphite (0001) surface energies (J/m^2)

Slab thickness	LDA US		LDA PAW	
	Classical σ	Boettger σ	Classical σ	Boettger σ
1	−0.760	X	0.077	X
2	−1.598	X	0.076	X
3	−2.435	0.077	0.077	0.076
4	−3.275	0.078	0.076	0.075
5	−4.113	0.079	0.079	0.077
6	−4.951	0.079	0.079	0.075
7	−5.788	0.079	0.075	0.074
8	−6.624	0.078	0.080	0.078
9	−7.468	0.076	0.078	0.075
10	−8.300	0.081	0.076	0.075
11	−9.146	0.074	0.081	0.078
12	−9.985	0.079	0.084	0.076
13	−10.824	0.079	0.082	0.074
14	−11.657	0.081	0.081	0.075
Std. dev.	X	0.0020	0.0026	0.0014

$$\text{Classical surface energy} = \frac{1}{2A}(E_{\text{surface}} - E_{\text{bulk}}) \tag{2}$$

The σ was also calculated using the Boettger [45] equation where N = number of atomic layers in the slab, H_n = energy of system n layers thick, and H_N = average of all the H_n values.

$$\text{Boettger surface energy} = \frac{1}{2A}\left[H_n - \frac{n}{2}(H_N - H_{N-2})\right] \tag{3}$$

The Boettger equation is seen less often in literature [46–49], and was derived in response to observations [50] that the classical σ diverges for certain surfaces, such as the surfaces of compounds and non-cubic materials. The two equations differ in that the classical equation uses energy values from two types of calculations: one on the bulk unit cell and one on the free surface; whereas the Boettger equation only uses energies from calculations of surface slabs. Therefore, the classical equation is most precise when energies from both slab and bulk calculations are accurate to the same order, making σ values highly sensitive to the PW cutoff, BZ sampling scheme, vacuum thickness, slab symmetry, and other simulation parameters.

The σ diverged linearly with slab thickness using the classical equation for the LDA US, but oscillates in the 0.075–0.085 J/m^2 range for the LDA PAW. These oscillations increase with slab thickness, so neither the PAW nor the US gives a truly converged σ using the classical equation. We attribute this to the inability of LDA to reproduce van der Waals bonding. Specifically, the graphite (0001) surface is formed by cleavage of van der Waals bonds. The energy of a surface is due to its

dangling bonds, so if LDA cannot reproduce van der Waals bonding, then it cannot correctly reproduce the "dangling bonds" on the (0001) surface, thereby invalidating the classical equation. The LDA is simulating the presence of some type of electron distribution at the surface, but we do not know what it is.

Using the Boettger equation, the PAW gives a σ that oscillates with thickness, except the oscillations are smaller and in the range of 0.074–0.080 J/m^2. The US gives a σ that oscillates with thickness in the same range of 0.074–0.081 J/m^2. The Boettger σ converges because the σ calculated at any slab thickness relies on a difference in energies between that slab thickness and the previous slab thickness. Therefore, any error in the electron distribution due to the free surface is included in all the terms in the Boettger equation. These errors cancel each other and the σ converged to a fixed value. The Boettger surface energies for the different slabs vary by less than 10%, so any of the thickness values is valid. Comparisons with literature properties are in Section 5.3.

The forces on the atoms were examined in the relaxed surface slabs to see if there were any patterns. For any slab thickness, the only non-zero forces were normal to the surface plane, and the largest values were always exhibited by atoms in the surface and sub-surface plane. We believe this is due to adjacent pairs of atoms that try to fill their dangling bonds and move closer together. The strong in-plane sp^2 covalent bonds prevent this from occurring, which results in higher residual forces at the surface. All forces in all slabs were less than $\pm$0.012 eV/Å for any slab thickness. For any plane, the forces on adjacent surface atoms are not identical in magnitude. Instead, the force on one atom is slightly more than the force on the adjacent atom. Atomic relaxation calculations was repeated on a 2-layer thick, 2×2 surface slab to see if any reconstructions or relaxations might be present on an extended surface. None were found; there was no change in atom positions, and forces on atoms were identical to that in the 1×1 surface of the same thickness.

5.2. Surface electronic structure

We have calculated the work function (Φ) and electron affinity (EA) of the graphite (0001) for each slab thickness. The Φ(EA) of a surface is the energy needed to take an electron from E_F (CB minimum) and place it in vacuum, where both values are obtained from the same calculation. Fig. 6 provides the DOS for the 14-layer slab as calculated by the LDA PAW, and in general, the DOS for all slabs with more than one plane were very similar to this, for either LDA PAW or US.

The electronic structure of these surface slabs mirrors closely that found in the bulk unit cell because all slabs showed a VB width of 19.4–19.6 eV, a CB width of 10.7–13.3 eV, and a zero band gap, which are very similar to

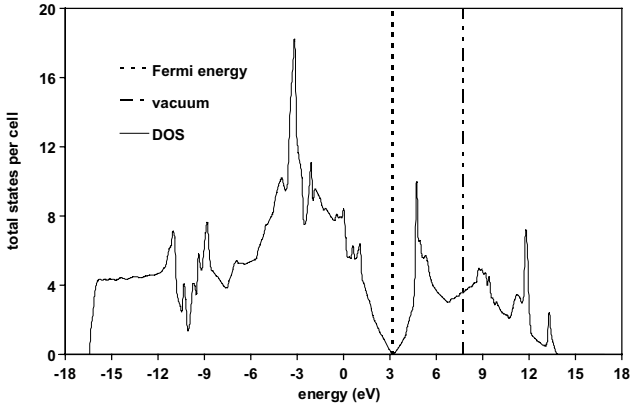

Fig. 6. DOS of the 14-layer graphite (0001) slab calculated by LDA PAW.

that seen in the bulk unit cell as calculated by all four XC + potential combinations. All slabs have a vacuum level inside the CB closer to the band minimum than to the band maximum, which mirrors that seen in the bulk LDA calculations. Because the graphite (0001) has a zero band gap, the $\Phi = EA$, and the calculated values fluctuated in the 4.4–5.2 eV range for different slab thicknesses for either PAW or US, reflecting the 2-D nature of its band diagram and electronic structure. Electronic properties of different slabs are given in Table 4; only the PAW data is listed as the US data are very similar.

The PDOS on different atoms in the 14-layer surface slab was compared to determine if there was a change in bonding between atoms at the surface and atoms in the slab middle away from the surface. There were minimal differences; peak widths and heights were in the same energy ranges. Like in the bulk, there was a small difference between the PDOS of a type 1 atom versus a type 2 atom such that the height of the $3p_Z$ peak changes slightly between the two atom types. In general, the PDOS of type 1 and type 2 atoms in the surface slab

Table 4
Graphite (0001) electronic properties (eV) using LDA PAW

Slab thickness	VB width	CB width	$EA = \Phi$
1	19.40	13.31	4.51
2	19.45	11.43	4.55
3	19.49	11.24	4.45
4	19.55	12.64	4.44
5	19.53	12.82	5.23
6	19.53	11.13	4.73
7	19.55	12.62	4.58
8	19.56	12.50	4.52
9	19.52	11.38	4.87
10	19.50	11.62	4.58
11	19.55	10.77	4.71
12	19.61	11.86	4.67
13	19.52	11.17	4.73
14	19.49	11.64	4.57

matched that found in the bulk unit cell, for both PAW and US. The slab one plane thick had a total DOS different from all the thicker slabs and from the bulk in that peak widths were the same, but the peak shapes were different (see Fig. 7). The peaks were closer together in height, and there were more of them than for the bulk or for thicker slabs.

The PDOS on either atom in the 1-layer slab were identical to each other in both the CB and VB, which contrasts with the bulk PDOS where type 1 and type 2 atoms had different peak shapes in the CB. This contrast supports our earlier conclusion that interaction in the 3p orbitals (which is manifested in different CB peaks for type 1 and type 2 atoms) partially accounts for interplanar bonding within the LDA–DFT model. The $3p_Z$ and $2p_Z$ contact at E_F, just like in the bulk, to give a semimetal.

The surface band diagram for the 1-layer slab was also analyzed, as shown below for the LDA PAW. The first, third, and higher odd-numbered bands are shown as dotted lines, and the solid lines are the even-numbered bands. The E_F is given as the horizontal line. The band diagram for the 1-layer slab was also obtained using the GGA PAW, and was essentially identical to that obtained using the LDA PAW, and so is not shown (see Fig. 8).

The surface band diagram has half as many occupied bands as that of the bulk, and this leads to several noticeable differences between the two. First, in the bulk band diagram, both $2p_Z$ bands contact both $3p_Z$ bands at E_F at the K point, and one $2p_Z$ and one $3p_Z$ band remain in contact throughout the entire H–K region. In the surface diagram, the sole $2p_Z$ band remains in contact with one sole $3p_Z$ band in the whole H–K region. The 1-layer surface has only type 2 atoms since there are no adjacent planes. From this, we conclude that the p_Z bands that contact at the H point only in the bulk band diagram are due to the electrons on the type 1 atoms, and that the p_Z bands that contact in the entire H–K region are due to electrons on the type 2 atoms. To our knowledge, no other publication has examined the electronic structure of a single, isolated graphene plane within the DFT formulism so we cannot compare these results with any others.

The band diagram was also obtained for an eight-layer surface slab using the LDA PAW, and a $15 \times 15 \times 2$ mesh of 135 k-points. This diagram can be compared with those previously obtained to see how the band structure and hence bonding changes going from an infinite bulk to a bulk crystal with free surfaces to a single graphene plane. This band diagram is very similar to that of the bulk and of the single plane; a semi-metal with the CB and VB touching with minimal overlap in the H–K region of the BZ. The similarities between the band diagrams of the bulk crystal, 1-layer and 8-layer slabs suggest that there are no electronic states created by the presence of a free surface. Like the results for the single layer of graphite, we could not find any other DFT calculation of the surface band diagram to compare our results with (see Fig. 9).

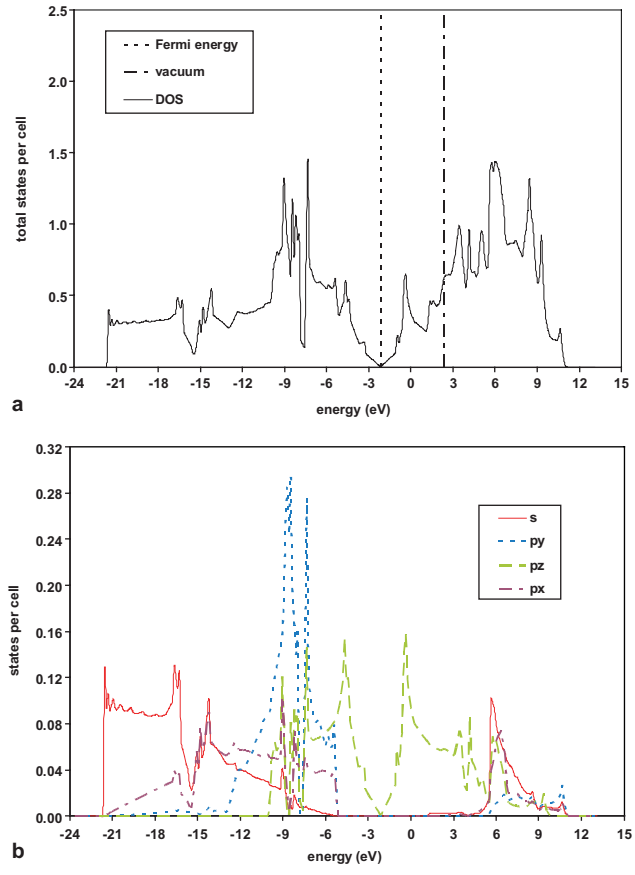

Fig. 7. DOS of the 1-layer graphite (0001) slab calculated by LDA PAW: (a) DOS for the whole slab and (b) projected DOS on either atom.

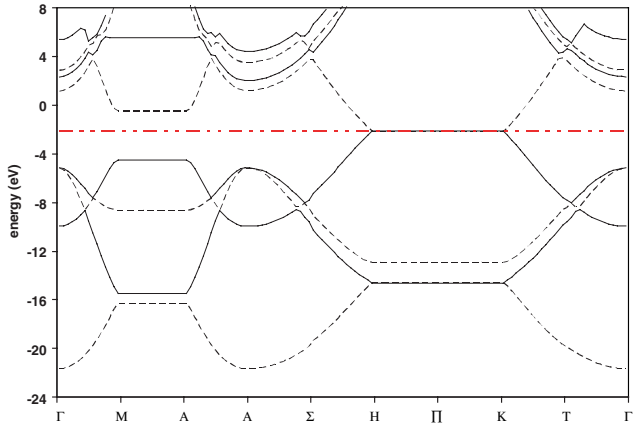

Fig. 8. LDA PAW band diagram for the 1-layer thick graphite (0001) slab.

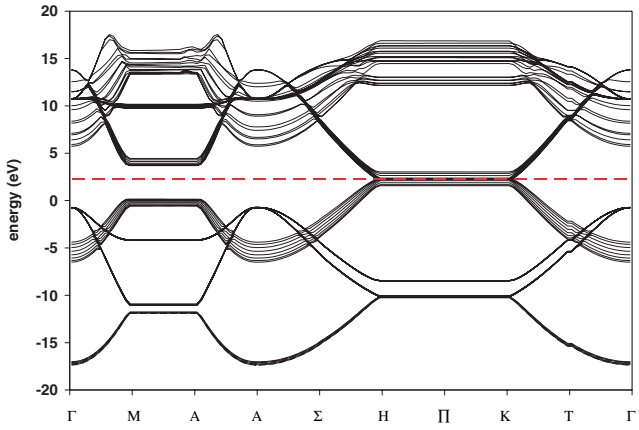

Fig. 9. Band diagram for an 8-layer surface slab: E_F is horizontal broken line.

5.3. Surface literature properties

The calculated value of $EA = \Phi = 4.4$–5.2 eV which coincides well with the 4–5 eV experimental range; see Table 5. Experimental EA values [51] exist for carbon clusters from 2–60 atoms in size and they show a general increase in EA with cluster size from 1.26 eV up to 4.1 eV for the largest clusters, which is in the range of our calculated values. For comparison, the clean diamond (1 1 1) surface has an experimental EA of 0.38 eV [52]. Our calculated VB widths are in the 19–20 eV range, which is just below the experimental range of 20–23 eV [53] and other calculated values [9]. We could find only one other DFT calculation of the (0 0 0 1) surface, Kern's thesis. Using VASP and Vanderbilt US PP, he calculated the σ as 0.0255 eV per 1×1 surface cell, or 0.079 J/m^2 using the Boettger equation. He did not calculate the classical σ and did not provide a reason why the Boettger equation was used instead of the classical equation, though we believe it is because he found a divergent classical σ as we did.

Table 5
Experimental graphite (0 0 0 1) values

Property	Source	Value	System	Method
σ	[54]	0.15 J/m^2	Pyrolytic	Sessile-drop experiment
σ	[55]	0.1–0.2 J/m^2	Pyrolytic	Sliding test
σ	Pierson	0.11 J/m^2	Not stated	Not stated
σ	[56]	0.03–0.2 J/m^2	Several types	Multiple methods
Φ	CRC	5.0 eV	Polycrystalline	Thermionic emission
Φ	[57]	4.35 eV	Not stated	Thermionic emission
Φ	[58]	4.7 eV	Not stated	Thermionic emission
Φ	[59]	4.48–4.88 eV	Not stated	Not stated
Φ	[60]	4.5 eV	Pyrolytic	Photoelectron spectr.
VB width	Heske et al.	19.6–22.2 eV	Several types	Photoelectron imaging

Experimental σ values are very small in magnitude, hence experimental variations lead to large relative differences. In general, these σ values are in the 0.03–0.2 J/m^2 range, and our calculations using the Boettger equation lie in this range; therefore we believe them to be reasonable. The σ of graphite is in some ways harder to experimentally measure than that of other materials due to the difficulty of synthesizing graphite to have near-ideal density; i.e. single crystal graphite. First, many atoms and molecules (i.e. water) easily intercalate within graphite by lodging between the basal planes thereby making the synthesis of pure graphite difficult. Second, anisotropic bonding in graphite promotes the formation of ribbons or an amorphous bulk over a single crystal. However, the only stable surface is the (0 0 0 1) basal plane, so any exposed surface of graphite will most likely be only the (0 0 0 1) facet.

6. Conclusions

We have examined the electronic and structural properties of hexagonal graphite using DFT with the LDA and GGA functionals. By construction, neither functional can reproduce dynamical van der Waals bonding in graphite. As a result, the GGA fails to reproduce interplanar bonding but the LDA does generate some sort of interplanar bonding and gives bulk properties similar to experimental values. Examination of the electronic structure by both functionals did not reveal any difference; hence the question of why the GGA fails for graphite remains unsolved. DFT–LDA calculations were then used to determine the geometry and electronic structure of the graphite (0 0 0 1). Surface energies obtained using two different pseudopotentials, the Vanderbilt US and the PAW, were on the order of 0.07–0.08 J/m^2. The graphite (0 0 0 1) does not exhibit any noticeable reconstructions or relaxations. The surface is semi-metallic, just like in the bulk, with the conduction and valence bands just touching, with minimal overlap. The work function and electron affinity were calculated to be equal to each other and in the range of 4.4–5.2 eV, which is in the range of available experimental values; with no theoretical data to compare with.

Acknowledgements

The authors acknowledge the National Center for Supercomputing Applications at the University of Illinois at Urbana Champaign for providing computational resources through grant number DMR000015N. We acknowledge the authors of VASP for help using and understanding the VASP software. We acknowledge

Louis Hector Jr. and Yue Qi at General Motors Research and Development Center, and members of the Computational Materials Science group at Arizona State University for help in performing calculations. We thank Timothy Terriberry for the free use of the VASP Data Viewer software [61]. This material is based upon work supported by the National Science Foundation under grant number 0101840. "Any opinions, findings, and conclusions or recommendations expressed in this material are those of the author(s) and do not necessarily reflect the views of the National Science Foundation."

Appendix 1. List of acronyms and synonyms

- DFT: density functional theory
- PP: pseudopotential
- PW: plane wave
- LDA: local density approximation
- GGA: generalized gradient approximation
- DLC: diamond-like carbon
- HOPG: highly-orientated pyrolytic graphite
- XC: exchange and correlation
- HF: Hartree Fock
- VASP: Vienna ab initio simulation package
- US: ultra-soft
- PAW: projector augmented-wave
- IBZ: irreducible Brillouin Zone
- H: enthalpy
- V: volume
- DOS: density of states
- PDOS: projected density of states
- VB: valence band
- CB: conduction band
- SPE: single point energy
- EA: electron affinity
- Φ: work function

References

[1] Gupta BK, Janting J, Sorensen G. Friction and wear characteristics of ion-beam modified graphite coatings. Tribol Int 1994;27(3):139–43.
[2] Shaji S, Radhakrishnan V. An investigation on surface grinding using graphite as lubricant. Int J Machine Tools Manufact 2002;42(6):733–40.
[3] Duncan DE. Sweat Tech Discover 2000;21(9).
[4] Ghorbani M, Mazaheri M, Khangholi K, Kharazi Y. Electrodeposition of graphite-brass coatings and characterization of the tribological properties. Surf Coat Technol 2001;148(1):71–6.
[5] Kelly BT. Physics of graphite. London: Applied Science Publishers; 1981.
[6] Girifalco LA, Hodak M. Van der Waals binding energies in graphitic structures. Phys Rev B 2002;65(12):125404–8.
[7] Rydberg H, Dion M, Jacobson N, Schroder E, Hyldgaard P, Simak SI, et al. Van der Waals density functional for layered structures. Phys Rev Lett 2003;91(12):126402–5.
[8] Lundqvist BI, Bogicevic A, Carling K, Dudiy SV, Gao S, Hartford J, et al. Density-functional bridge between surfaces and interfaces. Surf Sci 2001;493:253–70.
[9] Charlier JC, Gonze X, Michenaud JP. First-principles study of the stacking effect on the electronic properties of graphite(s). Carbon 1994;32(2):289–99.
[10] Furthmuller J, Hafner J, Kresse G. Ab initio calculation of the structural and electronic properties of carbon and boron nitride using ultrasoft pseudopotentials. Phys Rev B 1994;50(21):15606–22.
[11] Janotti A, Wei SH, Singh DJ. First-principles study of the stability of BN and C. Phys Rev B 2001;64(17):174107–11.
[12] Heske C, Treusch R, Himpsel FJ, Kakar S, Terminello LJ, Weyer HJ, et al. Band widening in graphite. Phys Rev B 1999;59(7):4680–4.
[13] Schabel MC, Martins JL. Energetics of interplanar binding in graphite. Phys Rev B 1992;46(11):7185–8.
[14] Wang Y, Scheerschmidt K, Gosele U. Theoretical investigations of bond properties in graphite and graphitic silicon. Phys Rev B 2000;61(19):12864–70.
[15] Boettger JC. All-electron full-potential calculation of the electronic band structure, elastic constants, and equation of state for graphite. Phys Rev B 1997;55(17):11202–11.
[16] Chen N, Yang RT. Ab initio molecular orbital calculation on graphite: selection of molecular system and model chemistry. Carbon 1998;36(7–8):1061–70.
[17] Butkus AM, Fink WH. Ab initio model calculations for graphite: bulk and basal plane electronic structure. J Chem Phys 1980;63(6):2884–92.
[18] Butkus AM, Fink WH. Ab initio model calculations of graphite: prismatic surface electronic density. J Chem Phys 1980;73(6):2893–8.
[19] Kresse G, Furthmuller J. Efficient iterative schemes for ab initio total-energy calculations using a plane wave basis set. Phys Rev B 1996;54(16):11169–85.
[20] Kresse G, Hafner J. Norm-conserving and ultrasoft pseudopotentials for first-row and transition elements. J Phys: Cond Matter Phys 1994;6(40):8245–57.
[21] Rappe AM, Rabe KM, Kaxiras E, Joannopoulos JD. Optimized pseudopotentials. Phys Rev B 1990;41(2):1227–30.
[22] Vanderbilt D. Soft self-consistent pseudopotentials in a generalized eigenvalue equation. Phys Rev B 1990;41(11):7892–5.
[23] Blochl PE. Projector augmented-wave method. Phys Rev B 1994;50(24):17953–79.
[24] Kresse G, Joubert D. From ultrasoft pseudopotentials to the projector augmented-wave method. Phys Rev B 1999;59(3):1758–75.
[25] Ceperley DM, Alder BJ. Ground state of the electron gas by a stochastic method. Phys Rev Lett 1980;45(7):566–9.
[26] Perdew JP, Chevary JA, Vosko SH, Jackson KA, Pederson MR, Singh DJ, et al. Atoms, molecules, solids, and surfaces: applications of the generalized gradient approximation for exchange and correlation. Phys Rev B 1992;46(11):6671–87.
[27] Pulay P. Convergence acceleration of iterative sequences: the case of scf iteration. Chem Phys Lett 1980;73:393–8.
[28] Broyden CG. A class of methods for solving nonlinear simultaneous equations. Mathematics of computation 1965;19:577–93.
[29] Johnson DD. Modified Broyden's method for accelerating convergence in self-consistent calculations. Phys Rev B 1988;38(18):12807–13.
[30] Press WH, Teukolsky SA, Vetterling WT, Flannery BP. Numerical recipes in FORTRAN 90: the art of parallel scientific computing. 2nd ed. Cambridge University Press; 1996.

[31] Polak E. Computational methods in optimization. New York: Academic Press; 1971.
[32] Hellman H. Einfuhrung in die Quantumchemie. Leipzig: Deuticke; 1937.
[33] Feynman RP. Forces in molecules. Phys Rev 1939;56:340–3.
[34] McKie D, McKie C. Essentials of crystallography. UK: Oxford Press; 1986. Pages 6–8.
[35] Birch F. Finite elastic strain of cubic crystals. Phys Rev 1947; 71:809–24.
[36] Blochl PE, Jepsen O, Andersen OK. Improved tetrahedron method for Brillouin-zone interactions. Phys Rev B 1994; 49(23):16223–33.
[37] Methfessel M, Paxton AT. High-precision sampling for Brillouin-zone integration in metals. Phys Rev B 1989;40(6):3616–21.
[38] Pierson HO. Handbook of carbon, graphite, diamond and fullerenes. USA: Noyes Publications; 1993. Page 51.
[39] Hanfland M, Beister H, Syassen K. Graphite under pressure: equation of state and first-order Raman modes. Phys Rev B 1989;39(17):12598–603.
[40] High temperature materials laboratory annual report, Oak Ridge National Laboratory 2000, p. 37.
[41] Brewer L. The cohesive energies of the elements. Lawrence Berkeley National Laboratory Reports, LBL-3720, 1977.
[42] Kern G. Ph.D. Thesis, Wien Technical University, Vienna, Austria 1998.
[43] Charlier JC, Gonze X, Michenaud JP. Graphite interplanar bonding: electronic delocalization and van der Waals interaction. Europhys Lett 1994;28(6):403–8.
[44] Mallett CP. The cellular method for graphite. J Phys C: Solid State Phys 1981;14:L213–20.
[45] Boettger JC. Non-convergence of surface energies obtained from thin-film calculations. Phys Rev B 1994;49(23):16798–800.
[46] Qi Y, Hector Jr LG. Adhesion and adhesive transfer at aluminum/diamond interfaces: a first-principles study. Phys Rev B 2004;69(23):235401–13.
[47] Siegel DJ, Hector Jr LG, Adams JB. Ab initio study of Al-ceramic interfacial adhesion. Phys Rev B 2003;67(9):092105–8.
[48] Marlo M, Milman V. Density-functional study of bulk and surface properties of titanium nitride using different exchange-correlation functionals. Phys Rev B 2000;62(4):2899–907.
[49] Vogtenhuber D, Podloucky R. Ab initio study of the $CoSi_2$ (1 1 0) surface. Phys Rev B 1997;55(16):10805–13.
[50] Fiorentini V, Methfessel M. Extracting convergent surface energies from slab calculations. J Phys: Cond Matter 1996;8(36): 6525–9.
[51] Lide DR, editor. CRC handbook of chemistry and physics. Cleveland, Ohio: CRC Press; 2004.
[52] Cui JB, Graupner R, Ristein J, Ley L. Electron affinity and band bending in single crystal diamond (1 1 1) surfaces. Diamond Related Mater 1999;8:748–53.
[53] Constanzo E, Faraci G, Pennisi AR, Terrasi A. Polycrystalline and highly oriented graphite: differences in the photoemission spectra. Solid State Commun 1990;74(9):909–12.
[54] Eustathopoulos N, Nicholas MG, Drevet B. Pergamon materials series: wettability at high temperatures. Amsterdam: Elsevier Science; 1999.
[55] Zaidi H, Robert F, Paulmier D. Influence of adsorbed gases on the surface energy of graphite: consequences on the friction behavior. Thin Solid Films 1995;264:46–51.
[56] Abrahamson J. The surface energies of graphite. Carbon 1975;11:337–62.
[57] Somorjai GA. Introduction to Surface Chemistry and Catalysis. USA: John Wiley & Sons; 1994. Page 381.
[58] Formenko VS. Handbook of thermionic properties. NY: Plenum Press; 1966.
[59] Reynolds WN. Physical properties of graphite. NY: Elsevier; 1968. Pages 113, 115.
[60] Moos G, Gahl C, Fasel R, Wolf M, Hertel T. Anisotropy of quasiparticle lifetimes and the role of disorder in graphite from ultrafast time-resolved photoemission spectroscopy. Phys Rev Lett 2001;87(26):267402–5.
[61] Terriberry TB, Cox DF, Bowman DA. A tool for the interactive 3D visualization of electronic structure in molecules and solids. Comput Chem 2002;26:313–9.